' 5$)7&23<□

Reduction in Defect Content in ODS Alloys – II

Interim Report on Contract 1DX-SY382V

J. Ritherdon and A.R. Jones

University of Liverpool, UK

Reduction in Defect Content in ODS Alloys – II

Interim Report on Contract 1DX-SY382V

J. Ritherdon and A.R. Jones

University of Liverpool, UK

1 Introduction

The work detailed within this report is a continuation of earlier work that was carried out under contract number 1DX-SY382V. The earlier work comprised a literature review of the sources and types of defects found principally in Fe-based ODS alloys together with a series of experiments designed to identify defects in ODS Fe_3Al material and recommend methods of defect reduction. Defects found in the Mechanically Alloyed (MA) ODS Fe_3Al included regions of incomplete MA, 'porosity', intrusions and fine-grained stringers. Some defects tended to be found in association with one another e.g. intrusions and fine-grained stringers. Preliminary powder separation experiments were also performed.

The scope and objectives of the present work were laid out in the technical proposal 'Reduction in Defect Content in ODS Alloys – II' which formed the basis of amendment 3 of the current contract. The current studies were devised in the context of the preceding work with a view to extending and concluding certain experiments while exploring new avenues of investigation of defect control and reduction where appropriate. All work proposed was within the context of achieving an ODS Fe_3Al alloy of improved overall quality and potential creep performance (particularly) in the consolidated, release condition. The interim outturn of the experimental work performed is reported in the following sections.

2 Factors controlling levels and distribution of porosity.

If the formation of micro-porosity is to be properly understood, its origin should be ascertained. To this end, TEM studies have been performed on samples of Fe_3Al from various stages in its manufacturing process; from the as-wrought powder to the consolidated alloy. The diversity of annealing response and microstructural change is illustrated.

FEG SEM studies of the secondary recrystallisation process provide quantitative analysis of the development of the secondary structure and investigate associations between grain structure evolution and the formation of porosity.

The degassing behaviour of Fe_3Al and PM2000 powders is compared and contrasted as hydrogen evolution is measured during degassing anneals. Work is in progress to accurately emulate the degassing regimes used by Plansee.

2.1 TEM of Fe_3Al powders.

TEM investigation of fully Mechanically Alloyed (MA) Fe_3Al powders was considered important in order to gain information on features that were likely to be below the resolution limit of FEG SEM and might play a role in the emergence of defects in subsequent stages of the consolidation and processing route. Features of potential interest included micro-porosity, dislocations, dispersoid particles and the as-wrought microstructure.

Electron-transparent samples of Fe_3Al powder were prepared in the following way:

- High concentrations of Fe_3Al powder were mixed with an epoxy resin.
- The mixture was packed into a 3mm O.D. thin-walled stainless steel tube and allowed to cure.
- Transverse "salami-like" slices approximately 0.5mm thick were cut from the filled tube and were mechanically polished to <100 micron thickness. The resulting discs of powder/epoxy were separated from their stainless steel outer and mounted on a copper grid.

- Mounted samples were thinned to electron transparency using a Gatan Precision Ion Polishing System (PIPS).

Samples were examined using a JEOL 2000FX TEM at an accelerating voltage of 200kV.

The intention is to check whether defects are confined to particular size fractions of the sieved powder or to specific powder annealing treatments. This presents a large matrix of possible experiments from which to choose a starting point. It was therefore decided to commence work using samples of Fe_3Al powder from the smallest and second largest size fractions and un-sieved powder which had been annealed to give complete recrystallisation.

Figures 1a and 1b show, respectively, a TEM micrograph of an as-wrought Fe_3Al powder particle from the <75micron sieved size fraction and an accompanying selected area diffraction pattern.

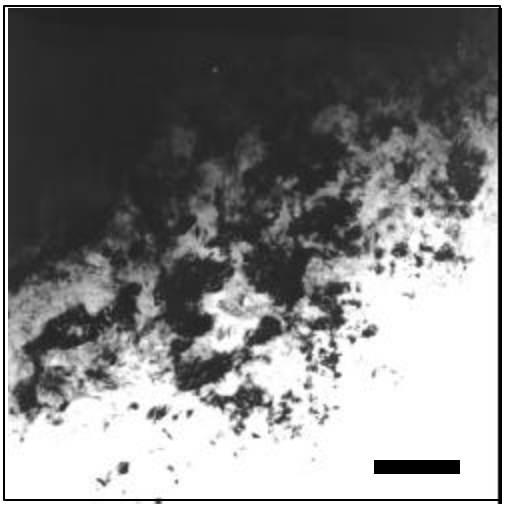

Figure 1a
TEM micrograph of an as-wrought Fe_3Al powder particle from the <75micron sieved fraction.

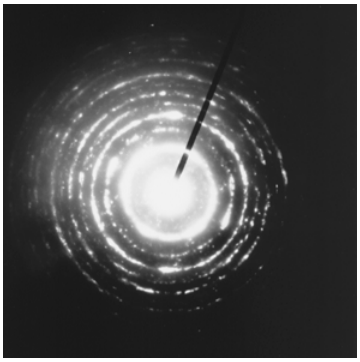

Figure 1b
Selected area (500nm aperture) diffraction pattern from an area such as that shown in Figure 1a.

The microstructure is clearly crystalline with a grain size of around 50nm. The diffraction pattern in Figure 1b shows a ferritic structure with a lattice parameter of 0.305 nm. Any lattice deformation due to elastic strain is evenly distributed throughout the region, as the diffraction rings are reasonably crisp and well defined.

TEM samples prepared from the second largest size fraction (>425 <600microns) of the Fe_3Al powder showed microstructures essentially similar to those in the <75micron powders although with some differences. Figures 2a and 2b show a TEM micrograph and its corresponding diffraction pattern, respectively.

It can be seen that the microstructure and SADP in Figs. 2a and b are generally similar to those shown in Figs. 1a and 1b. Figure 3a, however, shows that regions of extremely fine grain size (~5nm) also exist within the coarser powder fraction. The fine-grained nature of areas of this powder particle are confirmed by the diffraction pattern shown in Figure 3b, which exhibits an essentially continuous ring structure.

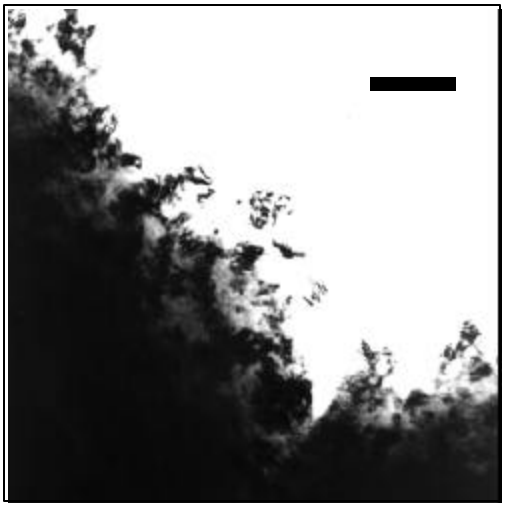

Figure 2a
TEM micrograph of an as-MA Fe_3Al powder particle from the >425 <600micron sieved fraction.

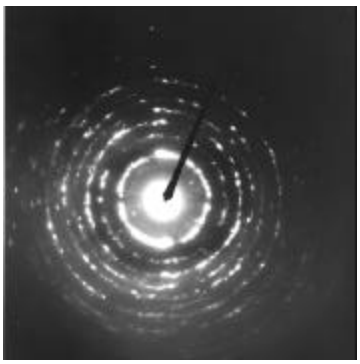

Figure 2b
Selected Area (500nm aperture) Diffraction Pattern (SADP) from the area shown in Figure 2a.

An additional feature apparent in Figure 3a is the 'layered' arrangement of the grain structure (arrowed). The origin of this grain morphology may be the folded structure commonly observed in fully processed MA powders. If it is related to the MA structure then the orientation of the 'layers' would vary throughout a powder particle and only certain regions would present the 'layers' edge-on to the section of the TEM sample. This may partly explain the infrequent observation of the 'layered' structure throughout the particle.

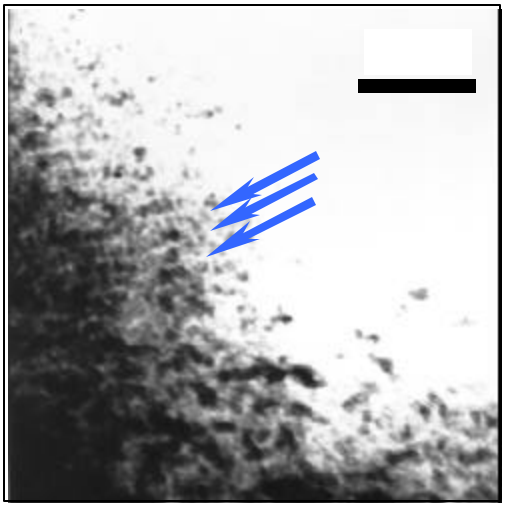

Figure 3a
TEM micrograph from a fine-grained region in an as-wrought Fe_3Al powder particle.

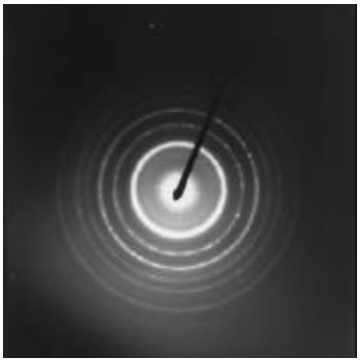

Figure 3b
Selected area diffraction pattern from the region shown in Figure 3a.

The differences in microstructure observed may be specific to different size fractions and caused by varying degrees of milling. However, at this stage, until more samples have been examined it is difficult to draw reliable conclusions from such differences as variation occurs between powder particles derived from the same sieved fraction.

A sample of un-sieved Fe_3Al powder was fully primary recrystallised by annealing for 1 hour at 900°C under vacuum. Although optical microscopy suggested that the powder had been fully recrystallised, TEM indicated otherwise. TEM of the microstructures of the fully recrystallised powder is shown in Figures 4a and 4b.

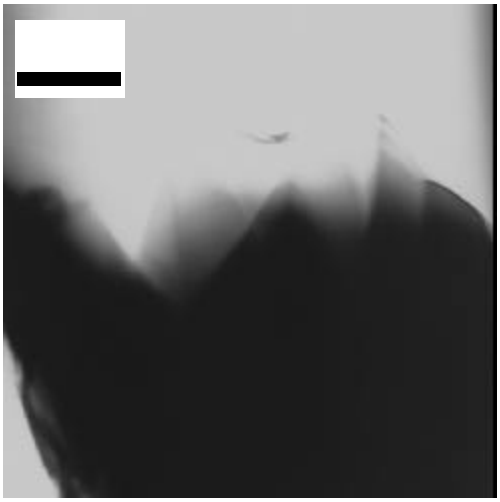

Figure 4a
TEM micrograph of coarse grains in a recrystallised sample of unseived Fe_3Al powder.

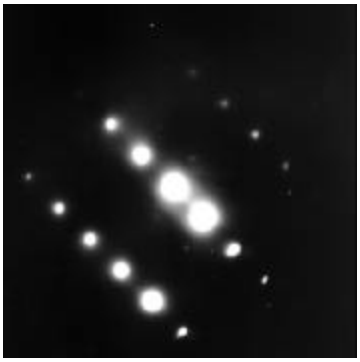

Figure 4b
Selected area diffraction pattern from the region shown in Figure 4a. ***B***=*<133>*

The grains shown in Figure 4a extended much further than the thin area of the sample and are therefore not well defined in the micrograph. However, the transformation is obvious if compared with a fine-grained region and it appears that primary recrystallisation of the powder has taken place in this area. The recrystallisation and grain growth also give rise to single crystal diffraction patterns from the selected area as shown in Figure 4b.
Perhaps surprisingly, recrystallisation was by no means as complete as had been suggested by optical microscopy. Figure 5a, for example, shows a fine-grained region with an associated 'layered' area similar to that seen in Figure 3a. The accompanying diffraction pattern (Fig. 5b) indicates a polycrystalline structure superimposed on a single crystal pattern.

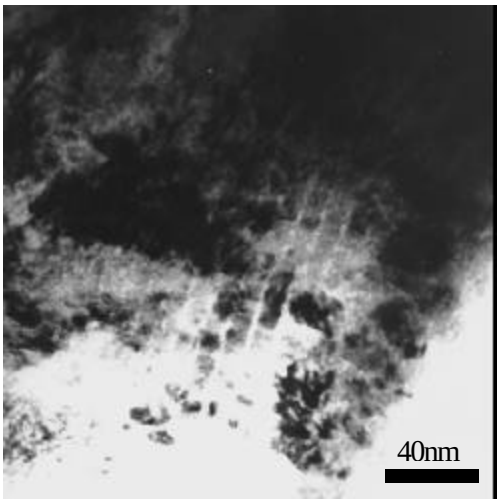

Figure 5a
TEM micrograph from an annealed and supposedly recrystallised sample of unseived Fe_3Al powder.

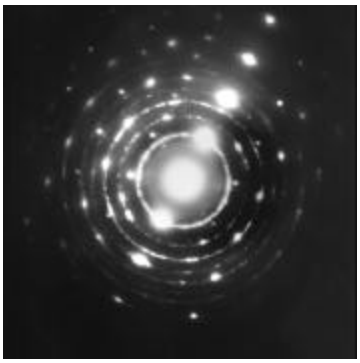

Figure 5b
Selected area diffraction patter from the region shown in Figure 5a. ***B***=*<113> (brightest spots)*

One explanation of this observation is an overlap of many fine grains and a recrystallising grain, although this is not clear in the image which highlights the fine-grained microstructure. In any case, coarse and fine grains exist in immediate proximity. The presence of such regions resistant to recrystallisation is surprising given the stored energy of deformation within the powers following MA. The observation suggests an inhomogeneous response to annealing exists in the Fe_3Al even at the powder stage.

Regions comprising only fine grains also existed in the ostensibly recrystallised sample as shown in Figures 6a and 6b. The diffraction rings in Figure 6b are extremely thick, suggesting that a range of lattice parameters based around the ferritic structure existed within the area analysed. When compared to other diffraction patterns, it can be seen that the thickening of the rings occurs only in the direction of the centre of the pattern, implying a range of lattice parameters greater than those measured from patterns with well-defined rings. Such a variation in lattice parameter may be due to a recovery or chemical homogenisation process although the change is contrary to that observed by XRD in annealed powders [Report No. ORNL/sub/98-SY382/01].

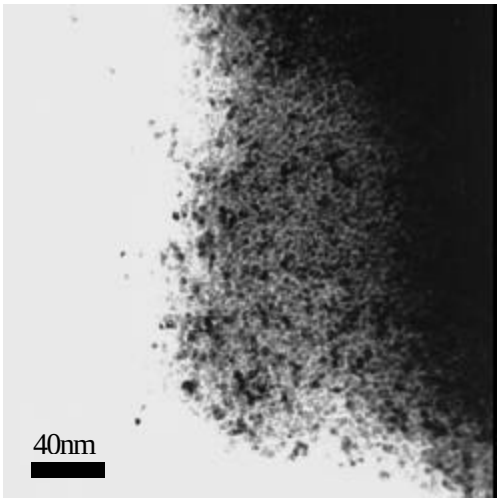

Figure 6a
TEM micrograph of a fine-grained region within an annealed Fe_3Al powder particle.

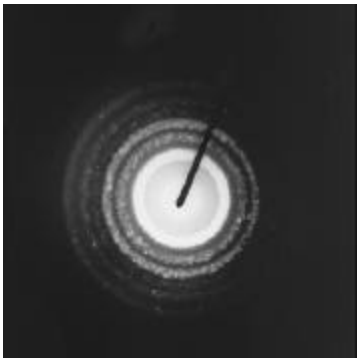

Figure 6b
Selected area diffraction pattern from the region shown in Figure 6a, showing the thick, polycrystalline ring pattern.

Overall, the powder appears to be still in the late stages of primary recrystallisation, as illustrated by the coexistence of both coarse- and fine-grained regions within the same particles. Figure 7 shows the interface between such coarse and fine grained regions at an advancing recrystallisation front.

TEM revealed that both recovery and recrystallisation are not nearly as complete as suggested by optical microscopy in these samples annealed at 900°C. It is perhaps surprising that these heavily deformed regions have resisted primary recrystallisation following annealing at these temperatures. While it is presently unclear why there should be such a range in the primary recrystallisation temperature of these powders (it was previously clear that Fe_3Al commenced recrystallisation at temperatures as low as 550°C),these observations do underscore the inherent variability in these materials even at the powder stage. Such variability may carry through to the consolidated alloy and influence the secondary recrystallisation process as well. Further work is necessary to understand more about the causes of this variability since it may be inherent to issues of quality control.

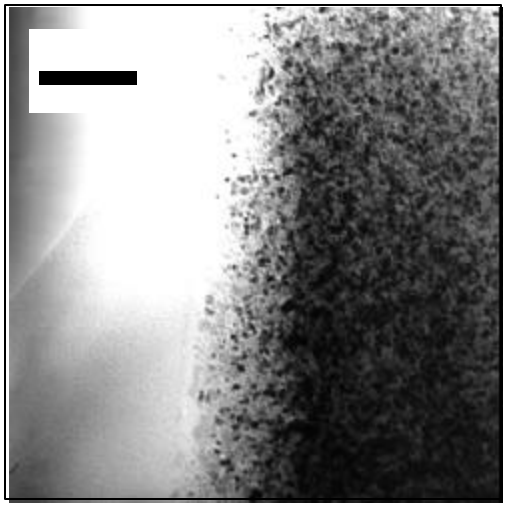

Figure 7
The interface between coarse- and fine-grained material in a recrystallising powder particle.

2.2 Microstructural evolution of secondary recrystallisation : Quantitative analysis

Both partially and 'fully' secondary recrystallised Fe_3Al have been studied in order to understand the likely origin and evolution of defects such as fine-grained stringers in the notionally fully secondary recrystallised state, as well as the development of porosity.

Samples of as-extruded Fe_3Al rod were annealed for 15, 30 and 45 minutes at 1275°C. These samples were examined together with and as-extruded material and material that had been 'fully' secondary recrystallised at ORNL.

Image analysis of channelling contrast FEG SEM photomicrographs from these annealed materials was performed either manually by superposition of a grid or using thresholded images and the image analysis program NIH Image 1.61.

2.2.1 Development of secondary recrystallised grain structures with annealing time.

The area fractions of primary and secondary recrystallised Fe_3Al were determined from FEG SEM images. These data are represented in Figure 8 as volume fractions of primary and secondary recrystallised material versus annealing time.

The volume fraction of secondary recrystallised material increased rapidly during the first 15 minutes of annealing thereafter approaching the 100% level asymptotically. Even after 45 minutes, only a few fine-grained primary recrystallised regions remained. Clearly, removal of any underlying microstructural heterogeneities which maintain such regions would result in significant reductions to the annealing time to achieve complete secondary recrystallisation at 1275°C.

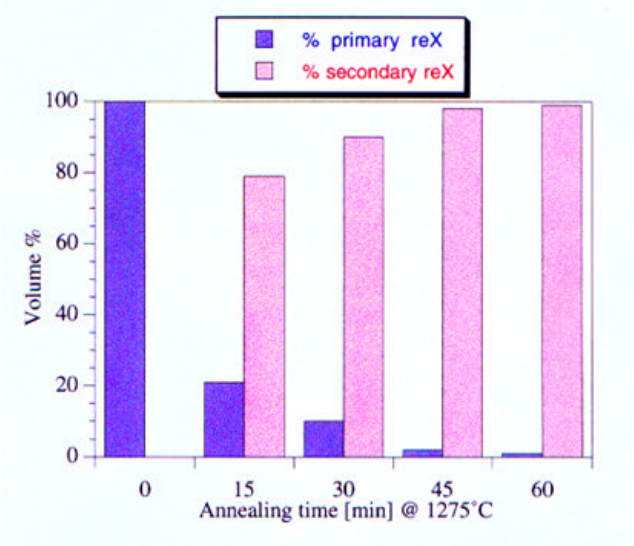

Figure 8
Volume fractions of primary and secondary recrystallised
Grain structures in Fe_3Al with progressive annealing time at 1275°C.

2.2.2 Evolution of pore size with secondary recrystallisation annealing time.

As mentioned in a previous report [Report No. ORNL/sub/98-SY382/01], much of the apparent porosity observed in polished sections of consolidated Fe_3Al can arise due to dissolution of the interface between the Al(O,N) particles and the alloy matrix by the alkali polishing medium, enabling these particles to drop out of the matrix. However, not all observed phenomena can be wholly explained by this dissolution effect. For example, there is a change in apparent pore size with annealing time as shown in Figure 9.

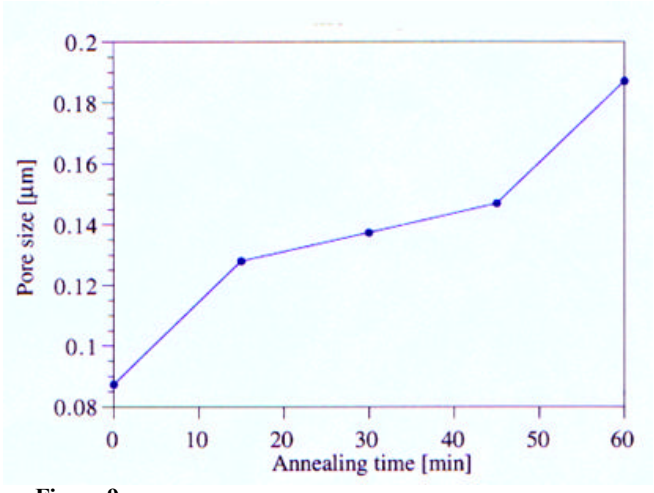

Figure 9
Change in pore size in consolidated Fe_3Al with
annealing time at 1275^0C.

The pore size increases by a factor of ≈2.5 between the as-extruded and 'fully' secondary recrystallised alloy. As it was felt that this might be due simply to softening of the alloy during annealing with correspondingly more rapid removal of material by the polishing

process, particularly at edges, the microhardness of the primary and secondary recrystallised areas was determined at different annealing times. The results are shown in Figure 10.

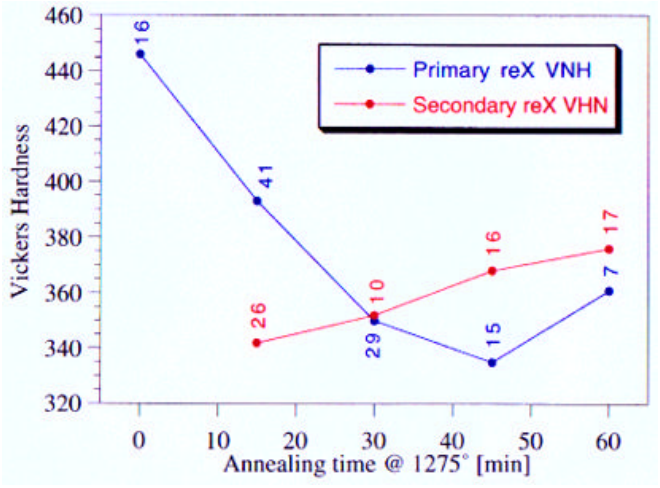

Figure 10
Change in microhardness (Vickers) of primary and secondary recrystallised material with annealing time. The standard deviation of each data point is shown.

The microhardness of the primary recrystallised regions does indeed drop significantly during the first 30 minutes of annealing. However, the levelling off of hardness at times greater than 30 minutes is not consistent with the continuously increasing pore size observed. Moreover, the hardness of the secondary recrystallised regions appears to increase with annealing time; again, inconsistent with an increase in pore size due to softening. It would seem, therefore, that coarsening of the size distribution of apparent pores is not due only to decreasing hardness but to other, as yet obscure, effects. Nevertheless, the data would suggest that not all the porosity effects are artefacts.

2.2.3 Pore spatial distribution in annealed samples.

The number and spatial distribution of pores in a given area were analysed in transverse sections of Fe_3Al samples after various annealing times at 1275^0C. The number of pores fluctuated at random around a value of 0.87 pores per square micron, showing no trend with annealing time. This seems to imply either that the pores are nucleated before or are associated with features that exist before secondary recrystallisation annealing. This is consistent with the previous observation that the pores are associated with Al(N,O) particles present immediately after consolidation.

The distribution of the pores was analysed and compared with a Poisson distribution to ascertain whether the pores were randomly distributed or existed in clusters. Figures 11a-e show the results of this comparison in terms of the number of pores that occur within the individual squares of a larger grid.

Superficially, the actual and Poisson distributions appear to match well as would be expected for a distribution of pores that is in the transverse section. However, χ^2 testing of curve fit is less conclusive, with good fit in some cases and poor fit in others. The implications of the χ^2 analysis is currently being assessed.

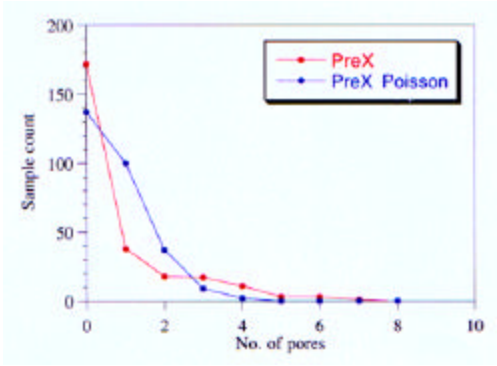

(a)

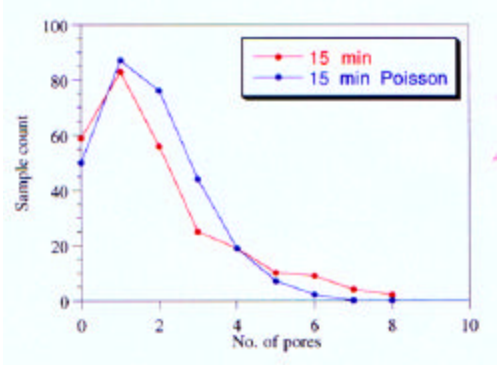

(b)

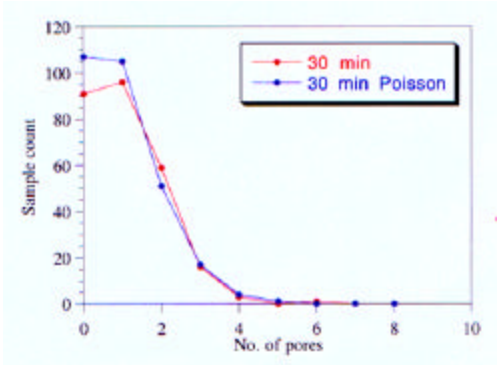

(c)

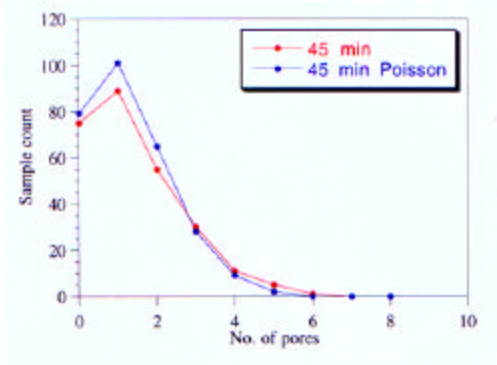

(d)

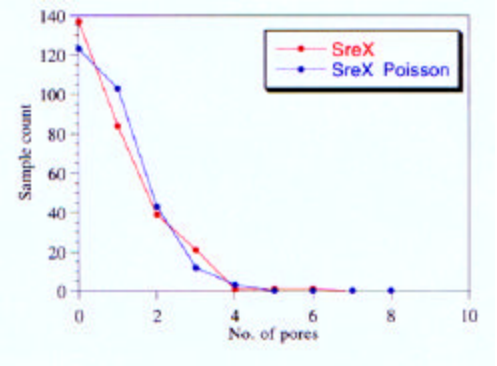

(e)

Figures 11a-e
Comparative plots of pore distributions and Poisson distributions at different annealing times.

These results imply that the distribution of pores (and therefore Al(N,O) particles) is random in the transverse section of consolidated Fe_3Al. In the longitudinal section the distribution is clearly not random as the pores/particles are arranged in loose stringers as previously reported [Report No. ORNL/sub/98-SY382/01].

2.2.4 Evolution of primary recrystallised grain size with annealing time.

The average grain size of the remaining primary recrystallised material was found to increase with annealing time, as shown in Figure 12. From the homogeneity of the grain size distributions, it seems that this slow coarsening is due to progressive normal grain growth driven by retained strain and grain boundary energy. No further study of this phenomenon was performed.

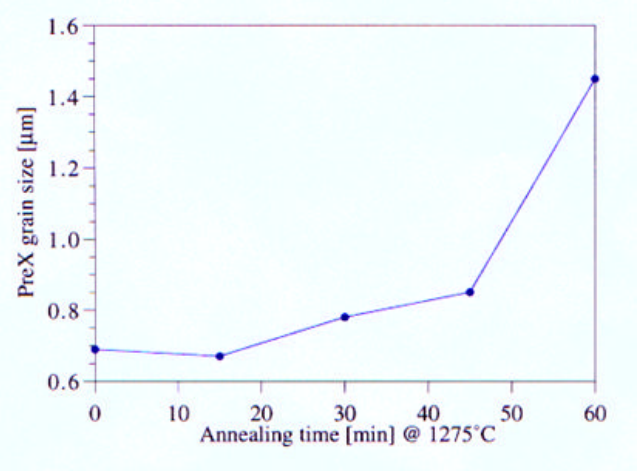

Figure 12
Increase in primary grain size with annealing time.

2.2.5 TEM analysis.

The fine-grained regions that remain in the ostensibly fully secondary recrystallised alloy are likely to be remnants of the primary recrystallised microstructure which, for some reason, have resisted the secondary recrystallisation process, having arrested the advancing secondary recrystallisation front. To ascertain whether or nor this is the case and to try to discover microstructural features which may explain this resistance to secondary recrystallisation, TEM specimens were prepared and studied from samples at different stages in the secondary recrystallisation process.

Examples of the initial, primary recrystallised microstructures can be seen in the longitudinal and transverse sections shown in Figures 13a-b, respectively.

The elongated morphology of the grain structure is seen in the longitudinal section. Pinned dislocations are visible at dispersoid particles.

After 15 minutes annealing at 1275°C, the majority of the sample had undergone secondary recrystallisation. The area of most interest for TEM examination was the interface between secondary and primary recrystallised regions.

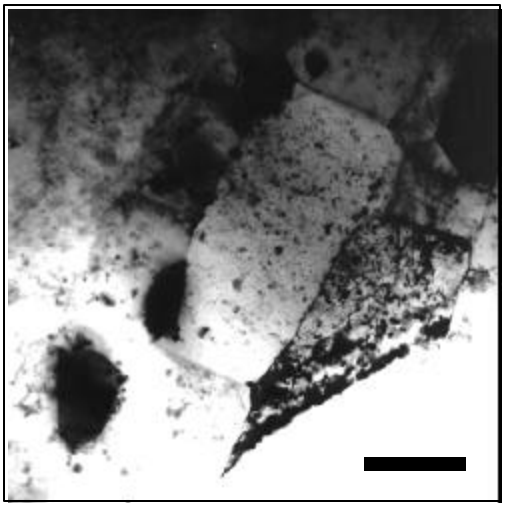

Figure 13a
TEM micrograph of a longitudinal section through primary recrystallised Fe_3Al bar.

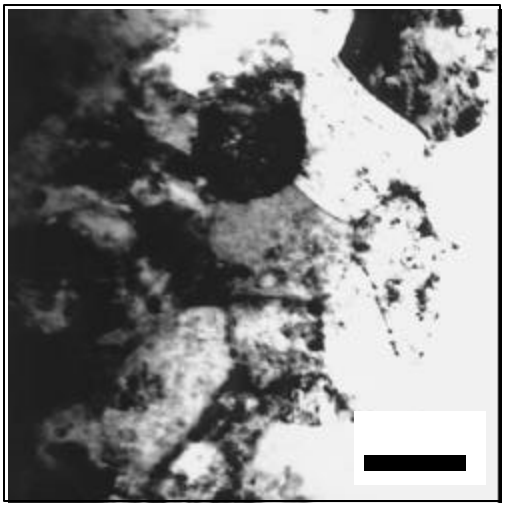

Figure 13b
TEM micrograph of a transverse section through primary recrystallised Fe_3Al bar.

Figure 14a shows such an interface in a longitudinal section with primary and secondary recrystallised material clearly visible. Also apparent are the loose stringers of Al(N,O) particles, which are particularly clear in the secondary recrystallised material. The secondary recrystallising interface can be seen to follow a line of particles for a few microns (arrowed) and then break away. Figure 14b also shows a longitudinal section, at higher magnification, and concentrates on the dispersoid and dislocation distribution in a primary recrystallised region. The middle region of the grain in the top of the micrograph can be seen to be almost dispersoid and dislocation free. In adjacent grains and at the extremities of this particular grain, the dispersoid concentration was higher and there was an associated higher concentration of pinned dislocations. Such dispersoid free regions in the alloy represent local regions of reduced driving force for secondary recrystallisation. However, the reduced driving force is to some extent counterbalanced by an associated reduction in boundary pinning.

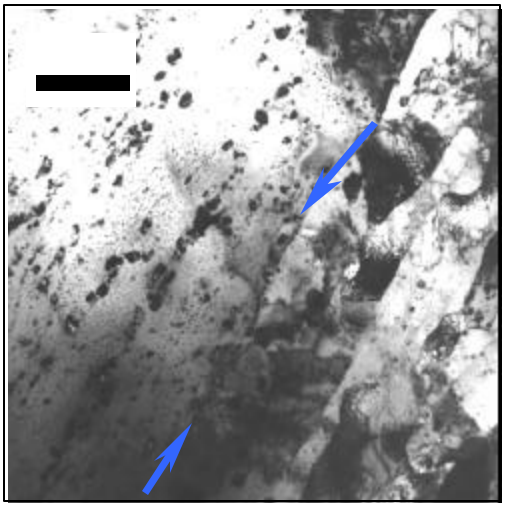

Figure 14a
TEM micrograph of the secondary recrystallisation interface in a longitudinal section of Fe_3Al annealed for 15 minutes at 1275°C.

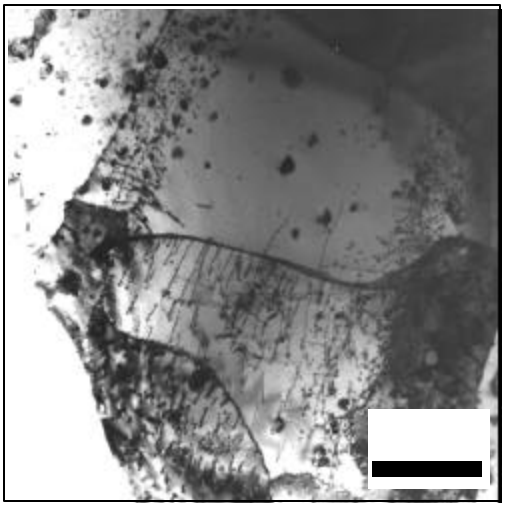

Figure 14b
TEM micrograph of the dislocation and dispersoid distribution in primary recrystallised grains of Fe_3Al annealed for 15 minutes at 1275°C.

Further evidence of Al(N,O) particle pinning effects at a secondary recrystallisation interface are shown in Fig. 15, taken from a transverse section.

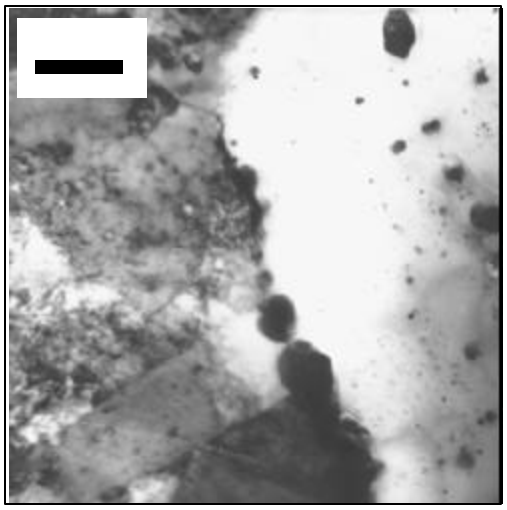

Figure 15
TEM micrograph of Al(N,O) particles along the secondary recrystallisation interface in a transverse section of Fe_3Al annealed for 15 minutes at 1275°C.

After 30 minutes annealing at 1275°C, more of the primary recrystallised material had been consumed but the secondary recrystallisation interface areas remained similar. See, for example, the transverse section in Fig. 16a. An interesting and possibly important feature discovered in secondary recrystallised material is shown in the longitudinal section presented in Fig. 16b.

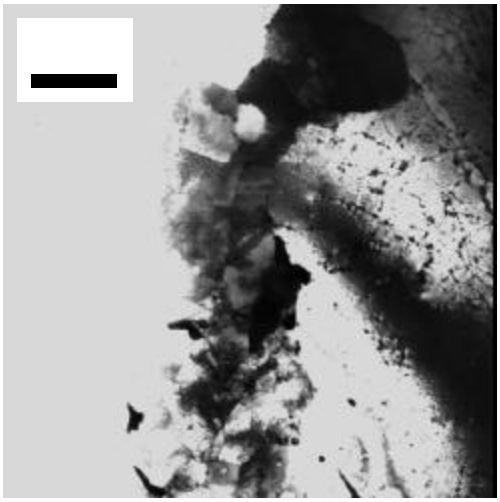

Figure 16a
TEM micrograph of a transverse section though consolidated Fe_3Al annealed for 30 minutes at 1275°C showing primary and secondary recrystallised material.

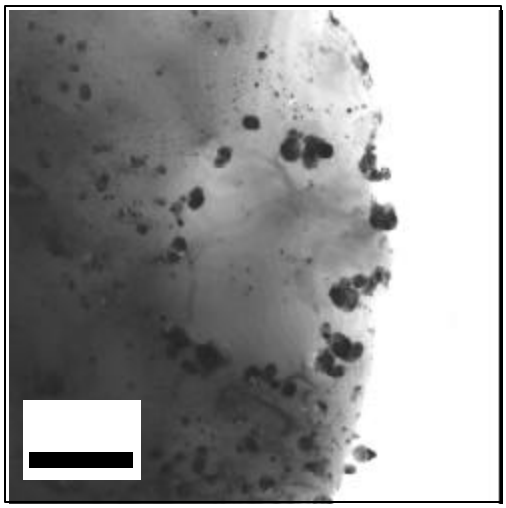

Figure 16b
TEM micrograph showing a 'loop' of Al(N,O) particles in secondary recrystallised material from a longitudinal section of Fe_3Al annealed for 30 minutes at 1275°C.

A concentration of Al(N,O) particles can be seen to describe a 'loop' surrounding material with a noticeably lower concentration of dispersoid particles. It seems likely that this concentration of aligned particles could represent the fragmented remains of surface oxide scale present on an individual primary powder particle prior to consolidation by extrusion.

Such evidence suggests that particularly deleterious spatial distributions of particles can pass through consolidation processes such as simple uniaxial extrusion relatively undisturbed, to unduly influence later thermomechanical processes.

At the TEM level, only the proportions of primary and secondary recrystallised material seemed to have altered after 45 minutes annealing at 1275°C. The transverse section in Fig. 17 showing the secondary recrystallised interface area is unremarkable, although the dispersoids and particles in the secondary recrystallised material near the interface do form intriguing patterns reminiscent of the 'loop' seen in Figure 16b. Also, some of the stringers of particles in the secondary recrystallised material coincide with grain boundaries in the primary recrystallised material at the recrystallisation interface.

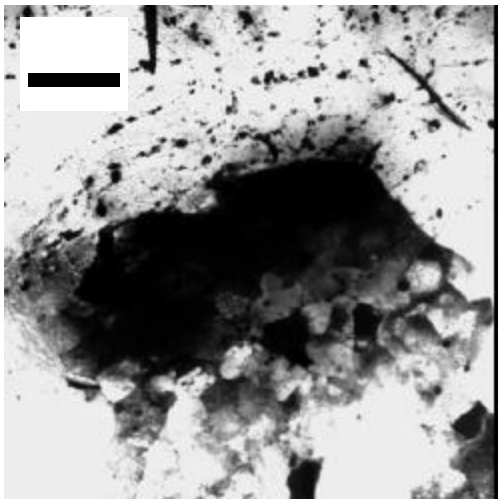

Figure 17
TEM micrograph showing a secondary recrystallised interface in a transverse section of Fe_3Al annealed for 45 minutes at 1275°C.

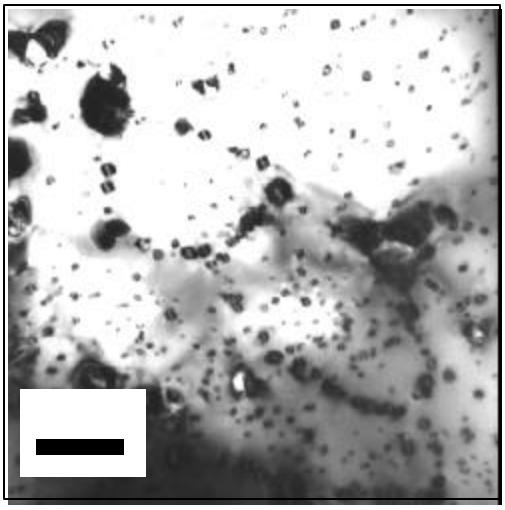

Figure 18
TEM micrograph of 'loops' of particles found in 'fully' secondary recrystallised Fe_3Al.

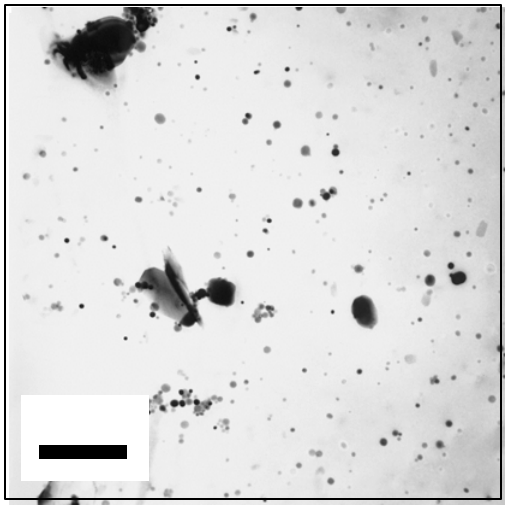

Figure 19
TEM micrograph of a transverse section through the alloy PM2000.

Remnant areas of secondary recrystallising interface in notionally 'fully' secondary recrystallised samples are difficult to locate, particularly given the restricted cross section represented by TEM samples. No images of reasonable quality have so far been obtained. Those areas that have been observed tend to imply that the interface area is much the same as in partially secondary recrystallised samples at shorter annealing times.

Figure 18 shows more spatially arranged 'loops' of particles observed in a secondary recrystallised region of a 'fully' secondary recrystallised sample of Fe_3Al. No such 'loops' have been observed in other ODS alloys such as PM2000. Figure 19 shows a typical view from a transverse section of PM2000 where there are generally fewer of the larger Al(N,O) particles and no loops of particles.

2.3 Degassing of Fe_3Al and PM2000 powders.

Further experiments on the degassing behaviour of both PM2000 and Fe_3Al powders have been continued in the current round of experiments.

Small quantities of powder (≈0.25g) have been heated in a tantalum boat that could be resistively raised to temperatures in excess of 1000°C within 3 minutes. A thermocouple was immersed in the powder and another spot-welded to the tantalum boat. This heating assembly was contained within a customised vacuum system, pumped by a diffusion pump and a sputter ion pump, at a pressure of $<10^{-9}$ mbar (at room temperature before heating). Total system pressure and partial gas pressures were measured using a VG Masstorr quadrupole mass spectrometer. The system pressure was also monitored with an ion gauge. The mass spectrometer and thermocouples can be connected to a PC via an A/D converter in order to improve sampling rate and accuracy.

2.3.1 Isothermal degassing.

A series of experiments has been performed in which small quantities of Fe_3Al and PM2000 powder were isothermally degassed at a range of temperatures and the hydrogen partial pressure measured with time. Results were plotted as partial pressure versus time and are shown below in Figures 20a-b.

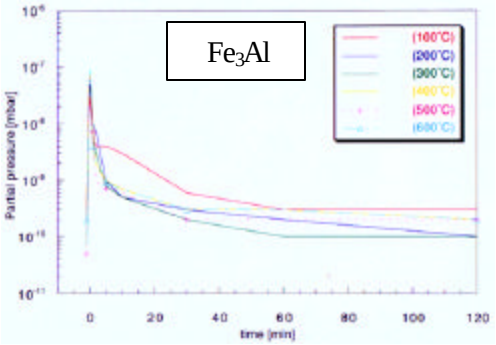

Figure 20a

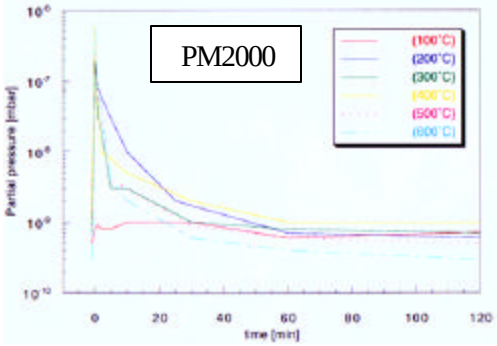

Figure 20b

Graphs of hydrogen partial pressure versus time for a) Fe_3Al and b) PM2000 powders isothermally degassed at a range of temperatures.

The form of the curves is essentially similar, with a peak in pressure on initial heating that tails off with time as the hydrogen was outgassed and pumped away. There are, however, two significant differences between the behaviour of the two powders.

Apart from the 100°C curve, the curves for Fe_3Al at all temperatures follow the same locus whereas the curves for PM2000 show a progressively steeper decline from the peak pressure as the temperature increases.

The PM2000 behaviour is presumably due to the increased degassing kinetics at higher temperatures. Hydrogen degassing behaviour of the Fe_3Al powder does not appear to be as temperature sensitive as that of the PM2000 and the overall volume of hydrogen given off is smaller.

The second difference between the Fe_3Al and PM2000 is that there does not appear to be any substantial gas evolution from PM2000 at 100°C whereas a strong peak is observed at this temperature for Fe_3Al. From these results it may be concluded that PM2000 requires a higher activation energy than does Fe_3Al, although it is not clear why this should be the case. In the next section, however, it is shown that the result for the Fe_3Al is anomalous and is probably due to experimental factors such as hot spots on the tantalum boat.

2.3.2 Outgassing with increasing temperature.

In order to elucidate the differences in hydrogen release kinetics exhibited in Fe_3Al and PM2000 powders, samples of powder were heated at a slowly increasing ($\approx 1°C.s^{-1}$) rate. The results were also compared to degassing of a chemically completely different powder: water-atomised pure copper. The hydrogen degassing results for all three powders are shown in Figure 21.

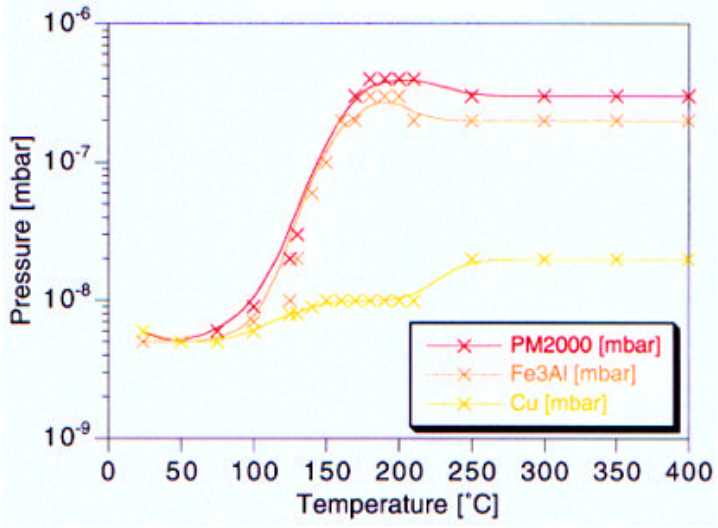

Figure 21
Hydrogen partial pressure versus temperature curves for Fe_3Al, PM2000 and pure Cu powder.
Heating rate »1°C.s^{-1}

As can be seen, the kinetic behaviour of the Fe_3Al and PM2000 powders is identical, although there does appear to be a greater amount of gas released from the PM2000. Both alloys require degassing temperatures to attain 110 - 120°C for significant amounts of hydrogen to be evolved. The data for Fe_3Al at 100°C in the previous section may therefore be assumed to be anomalous as mentioned.

The curve for the pure copper powder was relatively flat and any increase in hydrogen partial pressure was mirrored by a similar increase in total pressure caused by general degassing of the furnace during heating. The results gathered from the ODS powders are

therefore considered to be indicative of the powder behaviour and not due to experimental artefacts.

2.3.3 Total gas evolved.

In order to measure the total amount of hydrogen evolved from Fe_3Al and PM2000, the powders were heated up to 900°C in an evacuated but unpumped vacuum chamber and the rise in pressure recorded. Given that the quantity of powder is 0.25g, it is possible to obtain an estimate of the amount of hydrogen outgassed per gram of powder.

Preliminary results show that the quantity of gas evolved per gram of powder is $\approx 1.5 \times 10^{-8}$ mol. from Fe_3Al and $\approx 1.5 \times 10^{-7}$ mol from PM2000: a factor 10x higher in the PM2000.

This result vindicates the earlier observations that PM2000 outgases more than does Fe_3Al, and it is believed that as a comparison of powder behaviour the results are reliable. However, as an absolute measure of gas evolved, the results are still considered preliminary and prone to experimental error. The most notable possible sources of error are due to contributions to the system pressure from furnace outgassing and leaks, and that the pressure increase approaches the upper measurement limit for the apparatus used.

2.3.4 Plant degassing simulation.

A detailed schedule of the degassing treatment used by Plansee on the Fe_3Al MA powder has been obtained. Experimental procedure and apparatus are in the process of assembly so that the degassing treatment used at the Plansee plant can be simulated on a small scale in the laboratory. The intention is to ascertain what effects, other than hydrogen removal, this process has on the Fe_3Al powder. Powder particles will be examined before and after the degassing treatment.

It is believed that the origin of the large amount of particulate Al(N,O) found in consolidated Fe_3Al may lie at the degassing stage of manufacture where the unusually high amounts of aluminium in the alloy leave it open to the formation of a surface scale of aluminium oxide/nitride which fragments on consolidation and becomes entrained in the alloy. It may be therefore considered worthwhile to attempt to achieve adequate hydrogen removal from high aluminium alloys such as Fe_3Al by using more carefully tuned degassing treatments at lower temperatures than are presently employed.

2.3.5 Degassing summary.

Hydrogen is evolved from both Fe_3Al and PM2000 powders on heating, as would be expected. Kinetically, the outgassing processes appear identical in both alloy powders and an 'activation temperature' of around 110°C is required for outgassing to commence. However, there does appear to be some difference in behaviour in isothermal tests where Fe_3Al powders outgassed over a shorter time period than did PM2000.

It was found that, despite the similarities in kinetic behaviour, PM2000 powder outgases ten times as much hydrogen than does Fe_3Al.

There are two alternative conclusions that may be drawn from these results.

- More hydrogen in entrained within PM2000 powder during the MA process and therefore more is evolved during an outgassing anneal.

- Similar amounts of hydrogen exist within the as-MA Fe_3Al and PM2000 powders, but PM2000 powder releases its hydrogen more readily on annealing than does Fe_3Al powder.

The next step in this series of experiments is to determine the amounts of hydrogen contained by the two alloy powders prior to degassing. This information will clarify which of the above conclusions should be drawn.

3 Origin and control of fine-grained regions in secondary recrystallised structures.

3.1 Sieving of Fe_3Al and PM2000 powders.

Approximately 200g each of Fe_3Al and PM2000 as-alloyed powders were dry sieved and separated by powder particle size. The Fe_3Al powder (200.01g) was sieved in a vibrating stack with mesh sizes of 75, 150, 212, 425 and 600 microns. The PM2000 powder (200.04g) was similarly sieved but using mesh sizes of 75, 150, 212 and 300 microns. All fractions were weighed and retained. The resultant weight fractions are presented in Table 1.

Mesh size [µm]	Fe_3Al wt%	PM2000 wt%
>600	0.08	-
>425	0.96	-
>300	-	0.01
>212	2.15	0.06
>150	1.99	0.28
>75	14.23	1.30
<75	80.42	99.39

Table 1
Fractions of sieved powders expressed as percentages of the starting weight of the powders.
It may be noted that the percentages exceed 100%. This is due to the weighing of some impurities present in the sieves.

The fractions collected by the largest mesh sizes were studied to investigate whether they were significantly different to the bulk of the powder in any respect apart from size.

3.2 Particle morphology.

Large powder particles were mounted and studied by SEM. Micrographs of the ODS Fe_3Al and PM2000 powder particles are shown in Figs. 22a-b, respectively.

The Fe_3Al particle shown was typical of the largest powder fraction and showed severe cracking and splitting. Pockets packed with small powder particles are apparent on the particle surface. A small number of the largest particles looked more homogeneous and more like oversized versions of the standard sized particles.

Many of the PM2000 large particles were simply large but typical powder particles. However around 30% of the particles were of the form shown in Fig. 22b. They appear to be huge, generally flake shaped agglomerates of smaller particles.

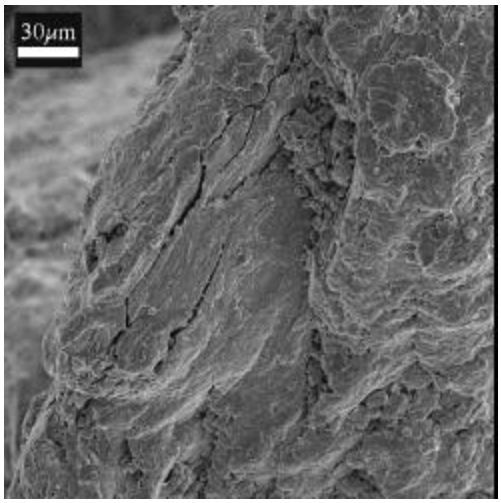

Figure 22a
SEM micrograph of abnormally large ODS Fe_3Al powder particle.

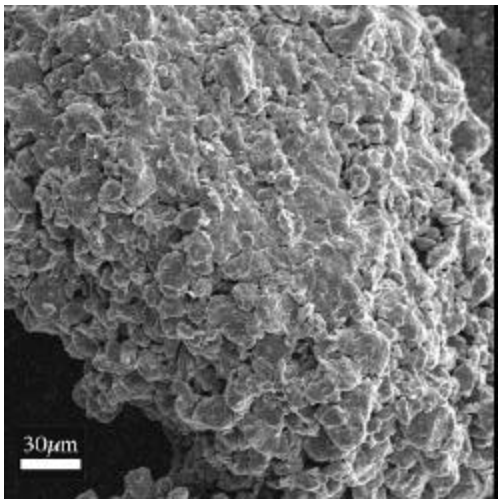

Figure 22b
SEM micrograph of abnormally large PM2000 powder particle.

Sectioned samples of the large Fe_3Al particles were prepared, etched and examined by optical microscopy to investigate the extent of the cracking apparent on the surface. One powder particle is shown at two different magnifications in Figures 23a-b. The cracking extended through the whole width of the particle including the fragmented inner regions. The mottled appearance of the alloy was due to etching of the micro-wrought MA structure of the alloy.

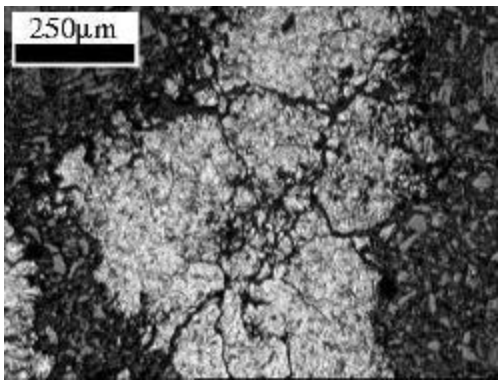

Figure 23a
Optical micrograph of a large Fe_3Al powder particle showing extensive cracking and fragmentation.

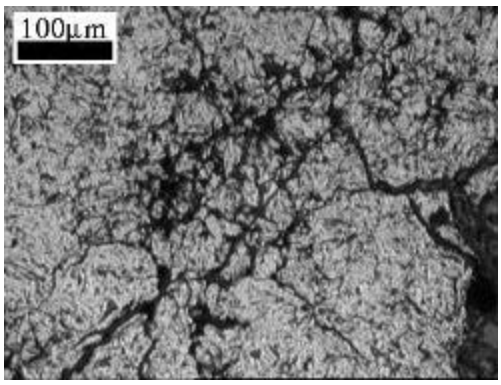

Figure 23b
Higher magnification of figure 23a.

3.3 Aluminium-depleted regions.

Transverse sections of the largest particle size fractions of Fe_3Al and PM2000 were prepared to a fine polish with negligible surface damage. These samples were examined in a FEG SEM in backscattered imaging mode to take high resolution SEM images, to check for areas of crystallinity via channelling contrast and to check for chemical inhomogeneity via the backscattering efficiency. Images are shown in Figures 24a-b below. The PM2000 micrograph shows the agglomeration of smaller particles and the bland, uniform contrast of the section through the homogeneously MA alloy. In the ODS Fe_3Al, cracking is apparent, as well as a fine distribution of bright regions. These bright regions are not obvious in a

secondary electron image of the same area and so are not due to channelling effects but to chemical differences and the resulting local change in backscattering coefficient.

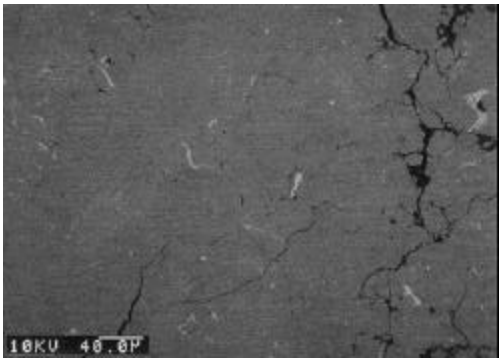

Figure 24a
Backscattered electron image of large Fe_3Al powder particle.

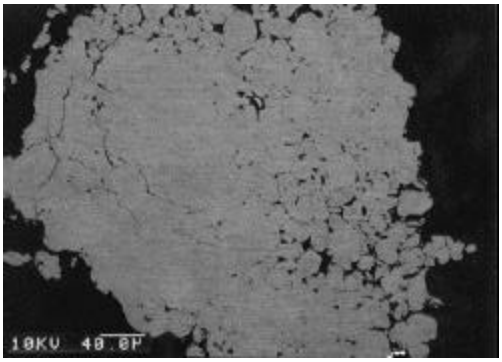

Figure 24b
Backscattered electron image of large PM2000 powder particle.

3.3.1 EDS analysis.

EDS analysis of the bright regions showed them to contain little or no aluminium, comprising instead only iron with a little chromium, as shown in Figure 25. The resulting increase in average atomic number gives rise to the enhanced back scattered electron contrast.

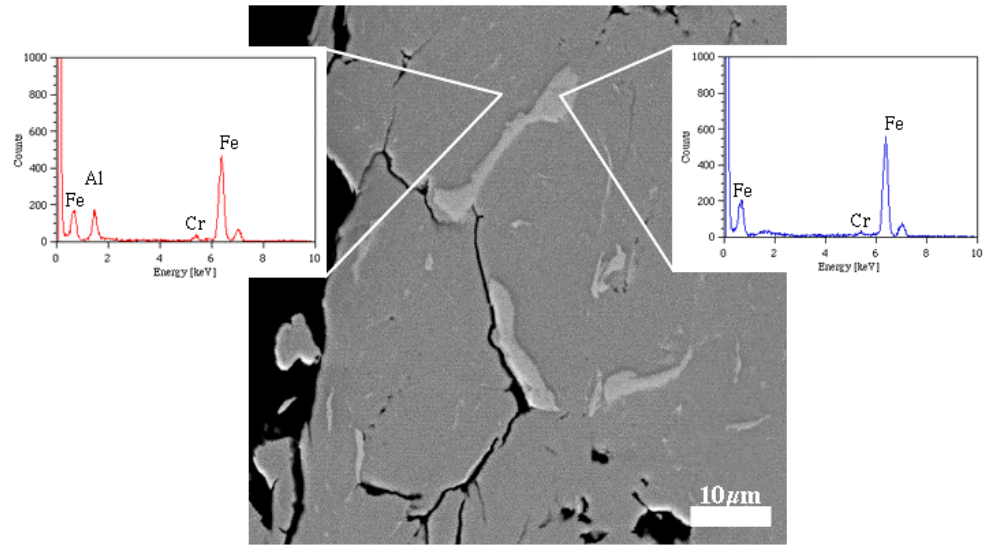

Figure 25
Backscattered electron image with corresponding EDS spectra from inhomogeneities in the largest Fe_3Al powder particles.

3.3.2 Electron microprobe analysis.

Energy dispersive microprobe analysis was used to obtain quantitative (with standards) analyses of the compositions of the aluminium-depleted inhomogeneities and the surrounding alloy matrix. The compositions of matrix and inhomogeneity from two powder particles are shown in Table 2.

As indicated by the preliminary EDS analyses, the aluminium levels found in the inhomogeneities were very low or negligible. The aluminium levels in the matrix are also much lower (40% lower) than those expected for this alloy.
The chromium levels in the inhomogeneities were approximately half of those in the matrix.

	Matrix Particle A	Inhomogeneity Particle A	Matrix Particle B	Inhomogeneity Particle B
Iron [wt %]	86.2	97.1	86.4	98.7
Aluminium [wt %]	11.1	1.2	11.0	0.1
Chromium [wt %]	2.7	1.7	2.6	1.2

Table 2
Electron microprobe analysis of two ADRs and the surrounding matrix.

3.3.3 Size and distribution.

Samples of powder from each size fraction were mounted, sectioned and polished and several backscattered electron images taken from each sample using SEM. These images were analysed to obtain data on the size and distribution of the aluminium depleted regions (ADRs).

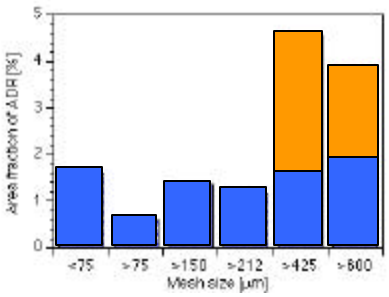

Figure 26
Plot showing area fractions of ADRs in different Fe_3Al powder size ranges. The ranges >425 and >600 microns in size contain extremely large ADRs.

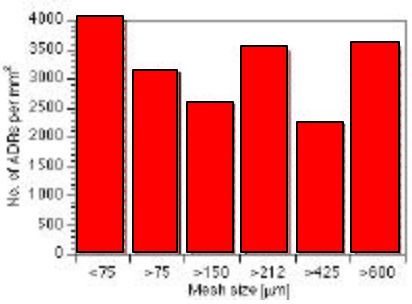

Figure 27
Plot showing the numbers of ADRs per mm^2 in different Fe_3Al powder size ranges.

Figure 26 shows the area fraction of ADR in different particle size ranges. The orange portions of the bars for the two largest size ranges show the effect that unusually large ADRs (>100µm) can have on the area fraction if included in the count. The blue bars represent data that include no such abnormally large ADRs from which it can be seen that generally the area fraction of ADR for each sample is not dependent on particle size. This implies that the overall amount of aluminium depleted material is similar in all size fractions.

Figure 27 shows the number of ADRs per unit area for the different size fractions. The plot does not show any obvious trend with particle size.

The implication of the above is that the overall degree of milling across the powder size range is reasonably constant with some notable exceptions. These exceptions occur when a massive ADR exists in a powder particle. Such ADR's dramatically increase the area fraction of aluminium depleted material in the particle without overtly affecting the number of ADR's per unit area. These particles have clearly undergone significantly less milling

than the majority of particles in the powder. This being so, they might be expected to contain little or no strengthening oxide (YAG) as well as little protective oxide forming aluminium.

3.3.4 Comparison with master alloy powder.

A sample of the pre-MA, gas-atomised master alloy powder was obtained and specimens prepared for SEM analysis in the whole and sectioned state. The objective was to determine whether or not the aluminium depleted inhomogeneities (ADRs) were present in the master alloy. The morphology of a typical master alloy powder particle is shown in Figure 28a.

The sectioned specimen was examined by SEM in backscattered mode so that many particles could be surveyed for chemical inhomogeneity in a reasonable time. No bright regions such as those observed in the MA powder were observed in the hundreds of particles surveyed. X-ray analysis of a more limited number (restricted to tens) of particles vindicated the backscattered SEM results, finding that the alloy had a composition similar to that expected. Two typical spectra collected from two different particles are shown in Figure 28b. X-ray analysis of the surface of particles showed similar results with a very small copper peak. The copper is of unknown origin but is considered insignificant at this stage.

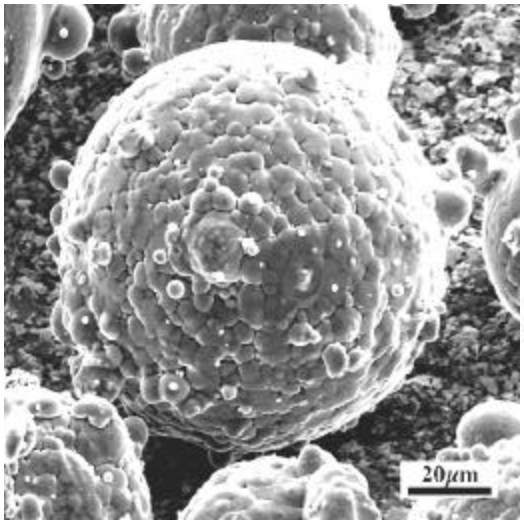

Figure 28a
SEM micrograph of a gas-atomised, pre-MA Fe_3Al master alloy powder particle.

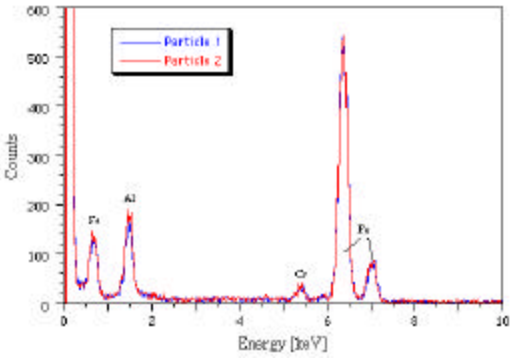

Figure 28b
X-ray spectra from sections of two master alloy powder particles similar to that shown in Figure 28a.

3.3.5 Quality control issues

Initially it was thought that the aluminium-depleted regions originated from the master alloy powder and had not been homogenized by thorough milling. It can be seen, however, that this is not the case and that the master alloy is homogeneous. This implies that aluminium-depleted regions were introduced or generated during the milling process. This could occur via processes such as contamination or aluminium depletion by selective oxidation.

A simple model approximating an ADR to a sphere of radius 75μm (not atypical for some of the larger depleted regions) shows that it has a similar volume to a 'cylindrical' fine-grained stringer of radius 15μm and length 2.5mm such as those observed in the 'fully'

secondary recrystallised consolidated alloy. This presents the reasonable possibility that ADRs and fine-grained stringers are linked, particularly considering the assumed low levels of MA in the ADRs and an associated low dispersoid concentration (previously observed in some fine grained stringers).

The low level of aluminium in the alloy matrix is peculiar and may well be restricted to the largest size fraction of powder particles. It is not clear how this arose and further analysis of individual powder particles from different size fractions of the MA powder is needed. One possibility is that aluminium-depleted fractions of the alloy may be more ductile and less susceptible to the fragmentation process of ball milling and therefore exist at a larger equilibrium size within the mill as dictated by the welding / fragmentation process.

If the worst of the observed anomalies are indeed restricted mainly to the largest size fractions of the MA powder then sieving to remove the largest size fractions ought to significantly reduce the proportion of microstructural inhomogeneities that lead to fine grained stringer defects in the secondary recrystallised condition. Moreover this should facilitate complete secondary recrystallisation at shorter times or lower temperatures than currently: either reducing unnecessary coarsening of YAG during the process. Sieving to remove all particles >425μm in size would result in the wastage of 1% by weight of the powder batch (see Table 1) and would eliminate the greatest regions of poor mechanical alloying. This size fraction could be re-cycled for re-milling, leading to more or less zero net loss in powder over a number of batches.

4 Fluidised bed powder separation trials.

Continued work, further to the trials already performed by the University of Groningen, Holland, was due to commence after some delay in September 1999.
By this date a comprehensive plan of action had been prepared in Liverpool and 20kg of free issue PM2000 powder received from Plansee GmbH had been shipped on to Holland.
However, due to technical difficulties involving the late manufacture and delivery of key components of the separation rig, the Dutch only began detailed experimental work towards the end of January 2000. Preliminary results are expected shortly.

It has been agreed with ORNL that Fe_3Al powder will be sieved before consolidation and the sieved fraction of large Fe_3Al powder particles will be shipped to Liverpool and then on to Holland to be used to 'seed' the PM2000 powder used for the separation experiments. The seeding will allow a known quantity of recognisable impurities to be added to the powder batch and subsequently separated, thus giving an accurate measure of the separation efficiency.

5 Specification of a production schedule for Fe_3Al with lower defect content.

In Section 3.5.5 recommendations are made for amendments to the Fe_3Al powder consolidation process whereby the bulk powder is sieved prior to consolidation in order to preclude certain size fractions that contain high proportions of defects.

Experimental work presently in progress detailed in Section 2.3.4 is designed to discover the origin of the high volume fraction of Al(N,O) particles in consolidated Fe_3Al. Using this data together with data already collected (Section 2.3.1 – 2.3.3), it is hoped that

recommendations for a revised degassing treatment will be devised to provide further reductions in alloy defect content.

6 Stimulation of interchange of non-confidential information, experience and materials between European and US ODS alloy programmes.

During the course of the programme proactive steps have been taken to encourage the interchange of information, experience and materials between various energy programmes.

An opportunity has been opened up for the exposure of trial samples of Fe_3Al material in a high temperature (currently up to 1100^0C) gasifier in a European (Sydkraft) biomass plant at Värnamo in Sweden. These trials will place the intermetallic samples alongside tubes of PM 2000 alloy from a European BRITE-Euram developmental project. It should be possible to negotiate exchange of data between these materials facilitating valuable comparative oxidation data in a field plant environment. A schematic of the Värnamo biomass plant is shown in Figure 29.

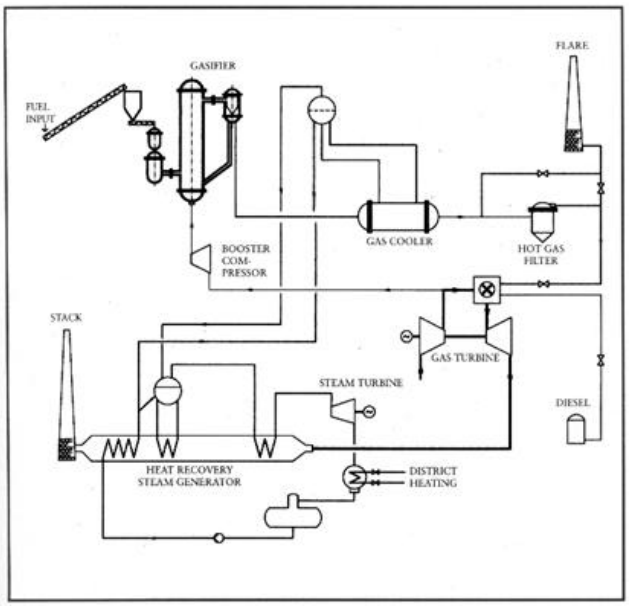

Figure 29
Schematic diagram of a biomass power generation plant.
By courtesy of Sydkraft AB, Sweden.

The gasifier is used to prepare combustible gases from pulverised wood fuel in a fluidised bed. Gasification takes place at temperatures around 950 - 1100°C and at a pressure of approximately 20 bar. Air is used as the gasifying medium and is supplied to the bottom of the gasifier at a temperature of 200- 250°C. A diagram of the Sydkraft gasifier illustrating the position of exposure samples is shown in Figure 30.

It is intended that Fe_3Al samples will soon be made available for insertion into the gasifier. The University of Liverpool is presently liaising between ORNL and Sycon (consulting arm of Sydkraft) to ascertain the sample specifications required by Sydkraft and how they compare with Fe_3Al product forms presently available at ORNL.

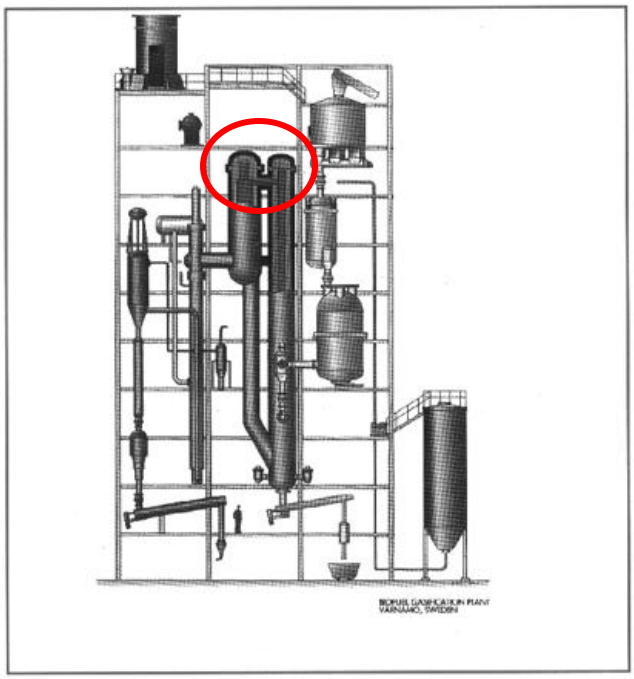

Figure 30
The Sydkraft gasification plant at Värnamo. [Approximately 40m high]
By courtesy of Sydkraft AB, Sweden.

7 Interim Conclusions.

ODS Fe_3Al powders have been examined by TEM in the as-MA condition (by sieve fraction size) and following annealing for 1 hour at 900^0C. Initial outturn suggests, perhaps unsurprisingly, that there is some variability in the microstructures found between powder particles. However, of more surprise is the apparent resistance shown by some powder particles to undergo subsequent recrystallisation from the very fine-grained as-MA condition. It has, for instance, been found that ODS Fe_3Al can commence recrystallisation at temperatures as low as 550^0C yet can contain individual powders still in an almost nanocrystalline condition following 1h annealing at 900^0C. Further work is being performed to understand these phenomena.

More sophisticated degassing trials have been performed on ODS Fe_3Al and PM 2000 powders in a custom vacuum system. These trials confirm earlier results indicating more hydrogen is released from the PM 2000 than the ODS Fe_3Al powders during degassing. In fact it is estimated that there is a factor ~10 difference in the amount of hydrogen released: $1.5x10^{-8}$ mol.gm^{-1} and $1.5x10^{-7}$ mol.gm^{-1} from the ODS Fe_3Al and PM 2000, respectively. What remains unclear at this stage, is very important and is being further investigated, is whether or not these differences in hydrogen released relate to differences in total hydrogen present in the two As-MA powders.

Detailed work has been performed to assess the differences in powder size distribution and as-MA powder quality as a function of different powder size fractions in ODS Fe_3Al and PM 2000. The work has shown that the PM 2000 powder occupies a much narrower size range (>99.3% all powders <75 μm mesh size) than ODS Fe_3Al powders. For the latter, some powder particles exceeded 600μm mesh size. Some of these larger powder particles appeared

to contain pockets of very fine powder in crevices around their periphery. Results also indicated that there are regions of apparently extraneous composition material entrained in the ODS Fe_3Al powders (principally Al-depleted) and that some of these identifiable regions can be substantial in size and appear to have resisted MA. Overall these results suggested there may well be a correlation between the deleterious fine grained stringers which can be retained following secondary recrystallisation and the retention of some of these larger ODS Fe_3Al powder particles. As a result it has been recommended that ODS Fe_3Al powders are sieved before consolidation to remove the approximately 1 wt.% of powder particles > 400μm in mesh size: these should be returned for re-MA. The origin of the regions of low Al level in the ODS Fe_3Al powders could not be traced to the master alloy. Further work on this issue is in hand.

Studies have been performed on the fully consolidated ODS Fe_3Al following both full and partial secondary recrystallisation anneals. It has been concluded that numbers of the pores observed, which coarsen in size by a factor of ~2.5 between consolidation and completion of the secondary recrystallisation anneal (1h / 1275^0C), are an artefact due to etching removal of Al(ON) particles. However, this is not the complete picture and it is considered that a proportion of the pores observed are likely to be genuine. Interim analysis suggests that the pore distribution is more or less spatially random in transverse sections of extruded rod, as opposed to the clear alignment of associated Al(ON) in stringers in longitudinal sections.
There is clear evidence that migration of the secondary recrystallising interface can be interrupted by stringers and concentrations of particles in the ODS Fe_3Al. Moreover comparison of transverse sections of ODS Fe_3Al and PM 2000 suggest there are higher concentrations of Al(ON) in the intermetallic alloy and these can be aligned even in the transverse section. It is felt these may well play a role in defining the ease with which secondary recrystallisation can be completed and the definition of final recrystallised grain boundary positions. Further work is in hand to establish the source of the differences in concentration and distribution of Al(ON) between the two alloy types. Specific lines of study are being pursued to this end.

Work to establish the potential for segregation powders using fluidised bed techniques has commenced. Results are expected shortly.

Opportunities have been established to expose coupons and samples of ODS Fe_3Al alloy at temperatures up to 1100^0C in the gasifier attached to a Swedish biomass power generation facility owned and operated by Sydkraft Värme AB. These samples would be exposed alongside PM 2000 alloy being exposed as part of a European funded BRITE-Euram project. It is likely that corrosion data from the biomass exposures can be exchanged between these projects.